Online Incremental Inductance Identification for Reluctance Synchronous Motors

Matteo Berto*, Luigi Alberti*, Floran Martin†, Marko Hinkkanen†
*Department of Industrial Engineering, University of Padova, Padova, Italy
†Department of Electrical Engineering and Automation, Aalto University, Finland

***Abstract*—The paper deals with the online incremental inductances estimation of a synchronous motor at low speeds using a high-frequency voltage injection. The control scheme is analogous to that used in position estimation algorithms, with the difference that the current control and the rotating voltage injection operate on the real dq axes. Thus a position sensor is required to apply this method. The corresponding current response is measured, filtered, and processed with an ellipse fitting technique. The estimated ellipse coefficients are then used to retrieve the incremental inductances online without the need of any post processing. A novel formulation to express the estimation error valid for other conventional signal injection techniques is presented. The method has been validated experimentally on a reluctance synchronous motor at locked rotor and during load and speed transients.**

***Index Terms*—Inductance, least squares, modeling, motor drives, permanent magnet motors.**

I. Introduction

PERMANENT magnet synchronous motors are widely adopted in variable speed drives for industrial applications due to their high torque density, dynamic performance, and efficiency. It is well known that synchronous reluctance motors (SynRM), permanent magnet assisted synchronous reluctance motors (PMA-SynRM) and interior permanent magnet synchronous motors (IPMSM) are usually characterized by nonlinear flux linkages maps [1]. As a consequence of that, the knowledge of an accurate model of the motor is necessary to design a high-performance current controller [2], [3]. Several parameter identification and self-commissioning methods for AC motor drives have been proposed in literature [4], [5], based on finite element simulations and laboratory measurements.

The focus of this paper is on the identification methods based on high-frequency (hf) voltage injection. In particular, an online incremental (differential) inductance estimation technique is proposed. The method is applicable to motors characterized by rotor saliency, i.e. reluctance and interior permanent magnet synchronous motors.

Ebersberger and Piepenbreier proposed a differential inductances and stator resistance identification method using test current instead of voltage injection [6]. A proportional-resonant controller located in parallel to each fundamental PI-type current controller in dq coordinates imposes a hf current injection. The hf-portions of the respective signals are separated online by means of the Goertzel algorithm and used to determine the differential self and mutual inductances. The main drawback of the method is that the test current signal injection cannot be executed simultaneously on both d and q axes. When the current signal is injected into the d-axis, the inductances l_{dd} and l_{qd} can be estimated. When the current signal is injected into the q-axis, the inductances l_{dq} and l_{qq} can be estimated. Another limit of the method is that its validity has been proved only at standstill (locked rotor).

Kuehl and Kennel proposed a method to estimate the differential inductances using a conventional pulsating voltage injection in dq superimposed to a sensored control scheme [7]. The differential inductances matrix is obtained measuring both the eigenvalues of the uncoupled inductance matrix and the estimation error ε from the sensorless algorithm. Similarly to [6] two separate measurements are necessary: one, where the sensorless algorithm tracks the estimated d-axis, and one for the q-axis. A post-processing least-squares optimization problem has to be solved to find the optimal correction variables. The method has been validated on an IPMSM coupled to a load motor, which was controlled at a fixed speed by an industrial inverter.

The identification method presented in this paper tries to extend the works in [6] and [7]. First of all, a rotating injection in dq allows to estimate simultaneously all the incremental inductances l_{dd}, l_{dq}, and l_{qq} without the necessity of perform two tests. Moreover, while the previous techniques were tested at locked rotor or at steady-state fixed speed, the presented online identification method is tested also during load and speed transients showing a good match with the expected inductances. The proposed method requires to solve an online least-squares problem (ellipse fitting) and presents innovative analytical equations that link estimation error and incremental inductances. Experimental tests validate the proposed method.

II. Considered Motor

The motor considered in this work is a 2-kW SynRM. The convention used to define d- and q-axis is depicted in Fig. 1, and the main data of the motor are shown in Table I. As concerns the flux linkages λ_{d} and λ_{q}, the motor has been characterized through experimental measurements [8]. The adopted characterization method required the use of a master motor to impose a speed of about 500 rpm. The flux linkages have been measured on a grid of stator currents $(i_{\mathrm{d}}, i_{\mathrm{q}})$ and then fitted with the algebraic model proposed in [9]. The model is particularly useful since it is possible to describe the SynRM nonlinear characteristics with only 9 coefficients, shown in Table II. The fitted flux linkages maps are depicted in Fig. 2.

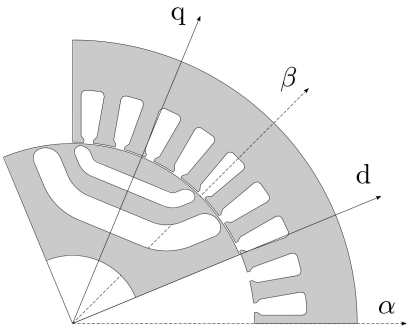

Fig. 1: Rotor and stator reference frames for SynRM.

TABLE I: Main data of the considered SynRM.

slots/poles	36/4	
rated power	2	kW
rated peak current	6	A
rated torque	16	Nm
rated speed	1400	rpm
stator resistance	4.6	Ω

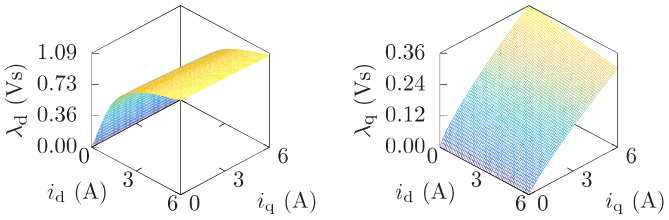

(a) d-axis flux linkage (b) q-axis flux linkage

Fig. 2: Measured flux linkages.

TABLE II: Fit coefficients for the considered SynRM.

coefficient	value		coefficient	value
a_{d0}	2.03	H^{-1}	S	5.42
a_{dd}	2.20		T	0.39
a_{dq}	12.83		U	1.90
a_{q0}	2.89	H^{-1}	V	0
a_{qq}	20.53			

The incremental inductances are defined and computed as follows:

$$l_{dd} = \frac{\partial \lambda_d}{\partial i_d} \tag{1a}$$

$$l_{dq} = \frac{\partial \lambda_d}{\partial i_q} = \frac{\partial \lambda_q}{\partial i_d} \tag{1b}$$

$$l_{qq} = \frac{\partial \lambda_q}{\partial i_q} \tag{1c}$$

where l_{dd} is the d-axis incremental inductance, l_{qq} the q-axis incremental inductance and l_{dq} the mutual incremental inductance - also known as cross-saturation inductance [10]. The so-computed incremental inductances (Fig. 3) will be used as a benchmark to validate the accuracy of the proposed identification method.

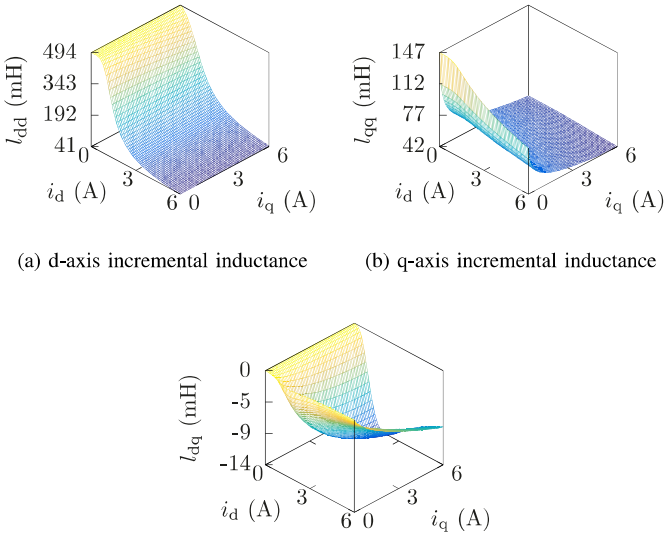

(a) d-axis incremental inductance (b) q-axis incremental inductance

(c) mutual incremental inductance

Fig. 3: Incremental inductances computed from the measured flux linkages.

III. High-Frequency Model

The proposed identification technique relies on hf voltage injection on d- and q- axis and real-time processing of the measured currents. In particular, a rotating injection on d- and q- axis is adopted. It is worth noticing that a position sensor (encoder or resolver) is required to inject the voltage signal on the real d- and q- axis. The d and q currents are measured, filtered, and processed online. The real-time processing consists of a least squares ellipse fitting and additional operations to compute the incremental inductances from the estimated ellipse coefficients.

The same assumptions for position estimation methods (based on saliency and signal injection) have to be verified. First of all, the proposed identification method can be used with motors characterized by rotor saliency, such as the SynRM, the PMA-SynRM and the IPMSM. Secondly, the frequency of the injected signals should be high enough to neglect the stator resistance effect on the estimation and, at the same time, the operating speed should be quite low (standstill or at the most 10% of the rated speed).

The hf model of a synchronous motor at quasi-zero speed is:

$$\begin{bmatrix} u_{hd}(t) \\ u_{hq}(t) \end{bmatrix} = \begin{bmatrix} l_{dd} & l_{dq} \\ l_{dq} & l_{qq} \end{bmatrix} \begin{bmatrix} \frac{\partial i_{hd}(t)}{\partial t} \\ \frac{\partial i_{hq}(t)}{\partial t} \end{bmatrix} \tag{2}$$

where u_{hd} and u_{hq} are the injected hf voltages and i_{hd} and i_{hq} the hf currents [11]. The adopted rotating voltage injection in the d- and q- axis is:

$$u_{hd}(t) = U_h \cos(\omega_h t) \tag{3a}$$

$$u_{hq}(t) = U_h \sin(\omega_h t) \tag{3b}$$

where U_h is the injection amplitude and $\omega_h = 2\pi f_h$, where f_h is the injection frequency. Once measured the stator currents

i_{d} and i_{q}, the hf currents $i_{h\mathrm{d}}$ and $i_{h\mathrm{q}}$ are obtained through high-pass filtering. The hf currents can be expressed as:

$$i_{h\mathrm{d}}(t) = \frac{U_h}{\omega_h(l_{\mathrm{dd}}\, l_{\mathrm{qq}} - l_{\mathrm{dq}}^2)} \left[l_{\mathrm{dq}}\, \cos(\omega_h t) + l_{\mathrm{qq}}\, \sin(\omega_h t)\right] \quad (4a)$$

$$i_{h\mathrm{q}}(t) = \frac{-U_h}{\omega_h(l_{\mathrm{dd}}\, l_{\mathrm{qq}} - l_{\mathrm{dq}}^2)} \left[l_{\mathrm{dd}}\, \cos(\omega_h t) + l_{\mathrm{dq}}\, \sin(\omega_h t)\right] \quad (4b)$$

or, in matrix form:

$$\begin{bmatrix} i_{h\mathrm{d}}(t) \\ i_{h\mathrm{q}}(t) \end{bmatrix} = \begin{bmatrix} \frac{U_h\, l_{\mathrm{dq}}}{\omega_h(l_{\mathrm{dq}}\, l_{\mathrm{qq}} - l_{\mathrm{dq}}^2)} & \frac{U_h\, l_{\mathrm{qq}}}{\omega_h(l_{\mathrm{dd}}\, l_{\mathrm{qq}} - l_{\mathrm{dq}}^2)} \\ \frac{-U_h\, l_{\mathrm{dd}}}{\omega_h(l_{\mathrm{dd}}\, l_{\mathrm{qq}} - l_{\mathrm{dq}}^2)} & \frac{-U_h\, l_{\mathrm{dq}}}{\omega_h(l_{\mathrm{dd}}\, l_{\mathrm{qq}} - l_{\mathrm{dq}}^2)} \end{bmatrix} \begin{bmatrix} \cos(\omega_h t) \\ \sin(\omega_h t) \end{bmatrix} \quad (5)$$

From (5) it is possible to obtain $\cos(\omega_h t)$ and $\sin(\omega_h t)$ as:

$$\cos(\omega_h t) = -\frac{\omega_h \left[l_{\mathrm{dq}}\, i_{h\mathrm{d}}(t) + l_{\mathrm{qq}}\, i_{h\mathrm{q}}(t)\right]}{U_h} \quad (6a)$$

$$\sin(\omega_h t) = \frac{\omega_h \left[l_{\mathrm{dd}}\, i_{h\mathrm{d}}(t) + l_{\mathrm{dq}}\, i_{h\mathrm{q}}(t)\right]}{U_h} \quad (6b)$$

The hf currents can be written in implicit form replacing (6) in $\cos^2(\omega_h t) + \sin^2(\omega_h t) = 1$ and collecting the ellipse coefficents. Finally, the hf ellipse can be written as:

$$a\, i_{h\mathrm{d}}(t)^2 + b\, i_{h\mathrm{d}}(t)\, i_{h\mathrm{q}}(t) + c\, i_{h\mathrm{q}}(t)^2 + f = 0 \quad (7)$$

where the coefficients a, b, c and f are:

$$a = l_{\mathrm{dd}}^2 + l_{\mathrm{dq}}^2 \quad (8a)$$

$$b = 2\, l_{\mathrm{dq}}\, (l_{\mathrm{dd}} + l_{\mathrm{qq}}) \quad (8b)$$

$$c = l_{\mathrm{qq}}^2 + l_{\mathrm{dq}}^2 \quad (8c)$$

$$f = -\frac{U_h^2}{\omega_h^2} \quad (8d)$$

The coefficients a, b, c depend on the operating point as well as the incremental inductances l_{dd}, l_{dq}, l_{qq}. On the other hand, the term f is constant if the injection amplitude and frequency U_h and f_h are not changed during an online operation.

Some additional parameters need to be introduced for the following analysis. The mean incremental inductance l_Σ and the semi-difference incremental inductance l_Δ are:

$$l_\Sigma = \frac{l_{\mathrm{qq}} + l_{\mathrm{dd}}}{2} \quad (9a)$$

$$l_\Delta = \frac{l_{\mathrm{qq}} - l_{\mathrm{dd}}}{2} \quad (9b)$$

The incremental inductance l_Σ is known to be related to the positive-sequence current response [12], [13]. On the other hand, the negative-sequence incremental inductance is:

$$l_{\mathrm{neg}} = \sqrt{l_\Delta^2 + l_{\mathrm{dq}}^2} \quad (10)$$

It can be seen that the terms l_Δ and l_{dq} are intrinsically linked in l_{neg}. The following analysis will focus on the separation of l_Δ from l_{dq}, a problem not yet addressed in literature. From now on, only the SynRM will be considered.

In order to split l_{neg} into l_Δ and l_{dq}, the knowledge of the estimation error ε (the error in the position estimation introduced by the cross-saturation effect [1]) is needed. The estimation error ε in the case of SynRM is defined as:

$$\varepsilon = \frac{1}{2}\, \mathrm{atan2}(l_{\mathrm{dq}}, -l_\Delta) \quad (11)$$

Applying the properties of the function $\mathrm{atan2}$, it is possible to re-write the estimation error with $\arctan$ as:

$$\varepsilon = \arctan\left(\frac{l_{\mathrm{dq}}}{-l_\Delta + l_{\mathrm{neg}}}\right) \quad (12)$$

This novel formulation can be exploited to compute:

$$\cos(\varepsilon) = \frac{1}{\sqrt{2}} \frac{-l_\Delta + l_{\mathrm{neg}}}{\sqrt{l_{\mathrm{neg}}^2 - l_\Delta\, l_{\mathrm{neg}}}} \quad (13a)$$

$$\sin(\varepsilon) = \frac{1}{\sqrt{2}} \frac{l_{\mathrm{dq}}}{\sqrt{l_{\mathrm{neg}}^2 - l_\Delta\, l_{\mathrm{neg}}}} \quad (13b)$$

The incremental inductances l_Δ and l_{dq} can be obtained from the incremental inductance l_{neg} and the estimation error ε with:

$$l_\Delta = l_{\mathrm{neg}}\, (1 - 2\cos^2(\varepsilon)) \quad (14a)$$

$$l_{\mathrm{dq}} = \sqrt{2}\, \sqrt{l_{\mathrm{neg}}^2 - l_\Delta\, l_{\mathrm{neg}}}\, \sin(\varepsilon) \quad (14b)$$

These equations are valid for other conventional signal injection methods as well, since the estimation error ε can be simply obtained subtracting the estimated position from the measured one during a sensored operation with the position observer in open loop. The proposed method, as will be explained in the following section, computes both l_{neg} and ε from the estimated ellipse coefficients a, b, and c.

IV. Proposed Method

The proposed control scheme is depicted in Fig. 4. A conventional control scheme with PI controllers is adopted. A position sensor is used to measure the rotor position and feed the Park transformation. The identification method consists of a hf voltage injection, an ellipse fitting procedure, and the high-pass (HPF) and low-pass (LPF) filters superimposed to the PI control scheme. In particular, a rotating voltage vector is injected, consisting of two pulsating phase-shifted signals in the d- and q- axis (3). A high-pass filter is adopted to extract the hf currents (4) which feed the ellipse fitting procedure. A low-pass filter is used to remove the hf component in the current control loop; however, the low-pass filter is not mandatory and it can even be removed [14].

An ellipse fitting procedure is used to estimate in real-time the ellipse coefficients a, b, c associated to the hf currents $i_{h\mathrm{d}}$ and $i_{h\mathrm{q}}$. The ellipse fitting of the current response locus has already been proposed in literature in the case of rotating injection in the stationary reference frame $\alpha\beta$ [15], [16]. The least squares problem associated to the ellipse fitting can be computational demanding if directly solved. Thus, a recursive solution method [15] and a recursive QR factorization technique [16] have been proposed in order the reduce the computational effort and guarantee the real-time operation of the ellipse fitting. Both methods can estimate the coefficients a, b, c of a rotating ellipse in $\alpha\beta$. The forgetting factor should accurately be tuned according to the rotating speed in order to guarantee a compromise between bias and variance estimation error [16].

The ellipse fitting is executed in dq in the proposed configuration. The main advantage of operating in dq is that

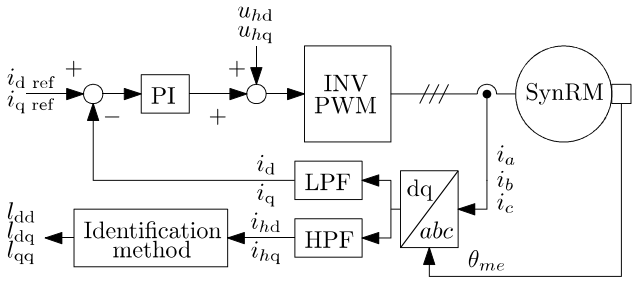

Fig. 4: Proposed identification method scheme.

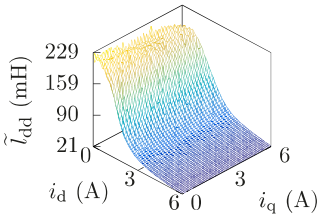

(a) d-axis incremental inductance

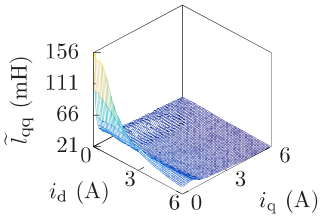

(b) q-axis incremental inductance

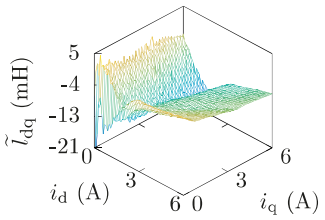

(c) mutual incremental inductance

Fig. 5: Estimated incremental inductances at $\theta_{me} = 0$ (first test).

a stationary ellipse can be detected, avoiding the speed-dependent forgetting factor tuning. As shown in Fig. 4, the i_{hd} and i_{hq} current samples are processed by the real-time fitting and the ellipse coefficients a, b, c are estimated. The estimated coefficients can be used to compute online the incremental inductances l_Σ and l_{neg}:

$$l_\Sigma = \frac{1}{2}\sqrt{a + c + \sqrt{4ac - b^2}} \tag{15a}$$

$$l_{\text{neg}} = \frac{1}{2}\sqrt{\frac{b^2 + (a-c)^2}{a + c + \sqrt{4ac - b^2}}} \tag{15b}$$

The coefficients a, b, c can be also used to compute ellipse tilt angle caused by the cross-saturation effect, which corresponds to the estimation error ε:

$$\varepsilon = \frac{1}{2}\,\text{atan2}(b,\, a - c) \tag{16}$$

The following step consists in splitting the negative-sequence incremental inductance l_{neg} (15b) into l_Δ and l_{dq} using the estimation error ε from (16). Equations (14) can be used for this purpose. The semi-difference incremental inductance l_Δ and the cross-saturation inductance l_{dq} are now available.

The last step consists in computing l_{dd} and l_{qq} using l_Σ estimated from (15a) and l_Δ:

$$l_{\text{dd}} = l_\Sigma - l_\Delta \tag{17a}$$

$$l_{\text{qq}} = l_\Sigma + l_\Delta \tag{17b}$$

The incremental inductances l_{dd}, l_{dq} and l_{qq} have been finally identified. The following section will focus on the accuracy of the identification method at standstill and during speed and load transients.

V. Experimental Results

The proposed identification method has been validated in two scenarios. The first test consisted of locking the rotor and analyzing the estimation accuracy in a grid of operating current points, while the second tests consisted of coupling the SynRM to a load motor and controlling the speed while varying the load torque. The experimental setup was composed by a dSPACE MicroLabBox and a three-phase inverter. The sampling frequency was set to f_c = 10 kHz. In both the tests the injected voltage had amplitude U_h = 40 V and frequency f_h = 1 kHz. These values appear to be adequate for the considered motor and the chosen sampling frequency. The following considerations have been drawn. The amplitude of the injected voltage U_h should be as low as possible in order to reduce acoustic noise and core losses, but it should be high enough in order to make the hf currents detectable and distinguishable from the current measurement noise. It has been verified that U_h = 40 V is a good compromise for the considered SynRM. Fixed the sampling frequency f_c, the injection frequency f_h must not be less than one fifth of f_c. In fact, the ratio between f_c and f_h corresponds to the number of points considered in the buffer of the ellipse fitting procedure. It is evident that the quality of the estimate increases with the number of points which constitute the circumference of the measured current ellipse. A buffer of 10 points, as the one adopted in the experimental tests, has been found satisfactory. As concerns the HPFs and LPFs, four digital first-order infinite impulse response (IIR) filters have been adopted [16]. The cut-off frequency has been set to 100 Hz for both HPFs and LPFs.

Fig. 5 shows the results of the first test with the rotor locked. The rotor has been locked with a mechanical brake at the position $\theta_{me} = 0$. The incremental inductances $\widetilde{l}_{\text{dd}}$, $\widetilde{l}_{\text{qq}}$ and $\widetilde{l}_{\text{dq}}$ have been estimated online and stored without the need of post processing. The algorithm has been tested on a grid of currents from 0 to 6 A, with a step of 0.1 A. The sequence of 61×61 reference currents $(i_{\text{d}}, i_{\text{q}})$ has been applied with the same pattern used in [17]. Considering a time step of 6 ms for each reference operating point, the total time required for the mapping was about 22 s. Fig. 6 shows the percentage error between the estimated incremental inductances at $\theta_{me} = 0$ (Fig. 5) and the incremental inductances obtained from the flux-linkage characterization performed at 500 rpm (Fig. 3). The accuracy of the method depends on the operating point. The $\widetilde{l}_{\text{dd}}$ percentage error is higher when the current i_{dd} is close to zero, while $\widetilde{l}_{\text{qq}}$ percentage error is around 40% in most of the considered current grid. Conversely, the $\widetilde{l}_{\text{dq}}$ percentage

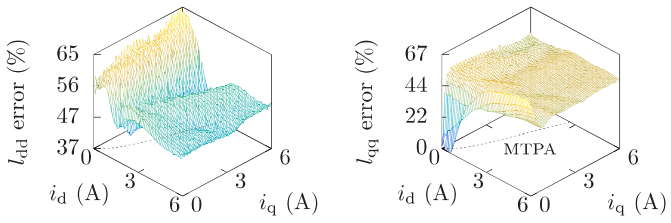

(a) $\widetilde{l}_{dd}$ percentage error

(b) $\widetilde{l}_{qq}$ percentage error

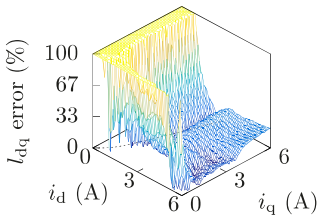

(c) $\widetilde{l}_{dq}$ percentage error

Fig. 6: Percentage error between the estimated incremental inductances at $\theta_{me} = 0$ (first test) and the incremental inductances obtained from the flux-linkage characterization performed at 500 rpm. The MTPA trajectory of the considered SynRM is shown in dashed line.

error appears to be remarkable along the dq axes and less than 30% at higher current values. The accuracy of the presented method can be assumed acceptable considering that all the estimation procedure can be carried on without knowledge of any motor parameters and without considering the effect of the rotor positon on the estimation. The accuracy of the method presented in [7], which is an offline and not online estimation, is between 10% and 20% depending on the operating point.

The results of the second test are reported in Fig. 7. The SynRM is coupled with a load motor which initially produces no torque. A 150-rpm speed reference step is set after 2 s from the beginning of the test, as shown in Fig. 7a. Then, a trapezoidal-shape load torque is imposed by the load motor maintaining the 150-rpm speed reference. The MTPA, shown in (Fig. 6), is the reference trajectory for the current control loop. The measured stator currents are depicted in Fig. 7b. The rated current amplitude of 6 A is reached during the load torque application. Fig. 7c, Fig. 7d and Fig. 7e show the online estimated inductances $\widetilde{l}_{dd}$, $\widetilde{l}_{qq}$, $\widetilde{l}_{dq}$ and the expected inductances l_{dd}, l_{qq}, l_{dq} during the whole test. It is worth noticing that, even during the load transients, the estimation accuracy is consistent with locked-rotor test (Fig. 5). Complementarily to the first standstill test, the method appears to be effective also during the second test characterized by a conventional operation. The chosen speed of 150 rpm can be assumed the upper limit for the considered SynRM for low speed signal injection techniques, consistently with the signal injection position estimation techniques which are usually valid up to a tenth of the rated motor speed.

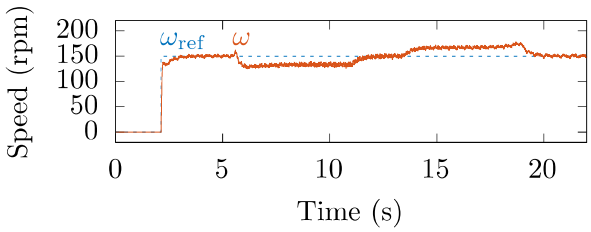

(a) Speed reference ω_{ref} and measured speed ω

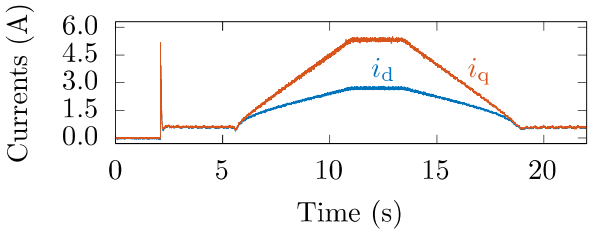

(b) Measured currents i_d and i_q

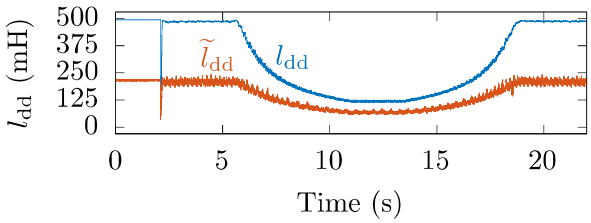

(c) Expected inductance l_{dd} and online estimated inductance $\widetilde{l}_{dd}$

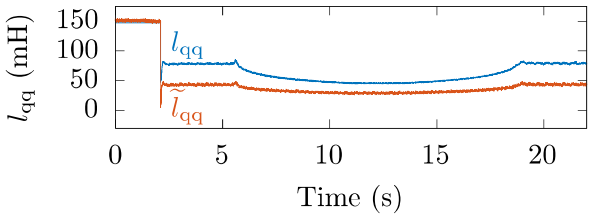

(d) Expected inductance l_{qq} and online estimated inductance $\widetilde{l}_{qq}$

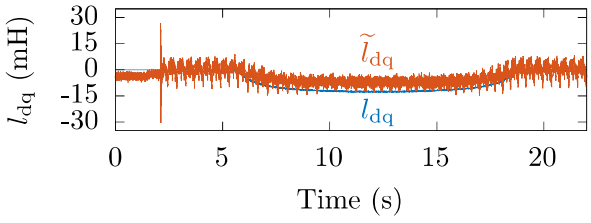

(e) Expected inductance l_{dq} and online estimated inductance $\widetilde{l}_{dq}$

Fig. 7: Results of the proposed identification method during speed and load transients (second test). The MTPA is the reference trajectory for the current control loop. l_{dd}, l_{qq}, l_{dq} are the incremental inductances obtained from the flux-linkage characterization, computed offline through lookup table. $\widetilde{l}_{dd}$, $\widetilde{l}_{qq}$, $\widetilde{l}_{dq}$ are the incremental inductances estimated online.

VI. Conclusion

The paper presents a novel identification method for reluctance and interior permanent magnet synchronous motors. The motor incremental inductances can be estimated online using a rotating high-frequency injection and a computationally efficient ellipse fitting. The relationship between the ellipse coefficients, the position estimation error and the incremental inductances are clearly explained and presented. The identification method has been tested on a SynRM both at standstill and during load and speed transients. The results are compared with a conventional flux linkages measurements technique.

Acknowledgment

This work was partially supported by the project "Green SEED: Design of more-electric tractors for a more sustainable agriculture" funded by Italian Ministry for University and Research with grant PRIN 2017SW5MRC.

References

[1] M. Berto, L. Alberti, V. Manzolini, and S. Bolognani, "Computation of self-sensing capabilities of synchronous machines for rotating high frequency voltage injection sensorless control," *IEEE Transactions on Industrial Electronics*, DOI 10.1109/TIE.2021.3071710, 2021, to be published.

[2] R. Antonello, L. Ortombina, F. Tinazzi, and M. Zigliotto, "Advanced current control of synchronous reluctance motors," in *2017 IEEE 12th International Conference on Power Electronics and Drive Systems (PEDS)*, DOI 10.1109/PEDS.2017.8289150, pp. 1,037–1,042, Dec. 2017.

[3] H. A. A. Awan, S. E. Saarakkala, and M. Hinkkanen, "Flux-linkage-based current control of saturated synchronous motors," *IEEE Transactions on Industry Applications*, vol. 55, DOI 10.1109/TIA.2019.2919258, no. 5, pp. 4762–4769, Sep. 2019.

[4] S. A. Odhano, P. Pescetto, H. A. A. Awan, M. Hinkkanen, G. Pellegrino, and R. Bojoi, "Parameter identification and self-commissioning in ac motor drives: A technology status review," *IEEE Transactions on Power Electronics*, vol. 34, DOI 10.1109/TPEL.2018.2856589, no. 4, pp. 3603–3614, Apr. 2019.

[5] M. S. Rafaq and J. Jung, "A comprehensive review of state-of-the-art parameter estimation techniques for permanent magnet synchronous motors in wide speed range," *IEEE Transactions on Industrial Informatics*, vol. 16, DOI 10.1109/TII.2019.2944413, no. 7, pp. 4747–4758, Jul. 2020.

[6] S. Ebersberger and B. Piepenbreier, "Identification of differential inductances of permanent magnet synchronous machines using test current signal injection," in *International Symposium on Power Electronics Power Electronics, Electrical Drives, Automation and Motion*, DOI 10.1109/SPEEDAM.2012.6264392, pp. 1342–1347, Jun. 2012.

[7] S. Kuehl and R. M. Kennel, "Measuring magnetic characteristics of synchronous machines by applying position estimation techniques," *IEEE Transactions on Industry Applications*, vol. 50, DOI 10.1109/TIA.2014.2322137, no. 6, pp. 3816–3824, Nov. 2014.

[8] E. Armando, R. I. Bojoi, P. Guglielmi, G. Pellegrino, and M. Pastorelli, "Experimental identification of the magnetic model of synchronous machines," *IEEE Transactions on Industry Applications*, vol. 49, DOI 10.1109/TIA.2013.2258876, no. 5, pp. 2116–2125, Sep. 2013.

[9] M. Hinkkanen, P. Pescetto, E. Mölsä, S. E. Saarakkala, G. Pellegrino, and R. Bojoi, "Sensorless self-commissioning of synchronous reluctance motors at standstill without rotor locking," *IEEE Transactions on Industry Applications*, vol. 53, DOI 10.1109/TIA.2016.2644624, no. 3, pp. 2120–2129, May. 2017.

[10] D. Mingardi, M. Morandin, S. Bolognani, and N. Bianchi, "On the proprieties of the differential cross-saturation inductance in synchronous machines," *IEEE Transactions on Industry Applications*, vol. 53, DOI 10.1109/TIA.2016.2622220, no. 2, pp. 991–1000, Mar. 2017.

[11] L. Alberti, N. Bianchi, and S. Bolognani, "High-frequency d-q model of synchronous machines for sensorless control," *IEEE Transactions on Industry Applications*, vol. 51, DOI 10.1109/TIA.2015.2428222, no. 5, pp. 3923–3931, Sep. 2015.

[12] F. Briz, M. W. Degner, A. Diez, and R. D. Lorenz, "Measuring, modeling, and decoupling of saturation-induced saliencies in carrier-signal injection-based sensorless ac drives," *IEEE Transactions on Industry Applications*, vol. 37, DOI 10.1109/28.952511, no. 5, pp. 1356–1364, Sep. 2001.

[13] J. M. Liu and Z. Q. Zhu, "Novel sensorless control strategy with injection of high-frequency pulsating carrier signal into stationary reference frame," *IEEE Transactions on Industry Applications*, vol. 50, DOI 10.1109/TIA.2013.2293000, no. 4, pp. 2574–2583, Jul. 2014.

[14] A. Piippo, M. Hinkkanen, and J. Luomi, "Sensorless control of pmsm drives using a combination of voltage model and hf signal injection," in *Conference Record of the 2004 IEEE Industry Applications Conference, 2004. 39th IAS Annual Meeting.*, vol. 2, DOI 10.1109/IAS.2004.1348530, pp. 964–970 vol.2, Oct. 2004.

[15] M. Berto, P. G. Carlet, V. Manzolini, and L. Alberti, "An effective ellipse fitting technique of the current response locus to rotating hf voltage injection in ipmsm for sensorless rotor position estimation," in *IECON 2018 - 44th Annual Conference of the IEEE Industrial Electronics Society*, DOI 10.1109/IECON.2018.8591855, pp. 391–396, Oct. 2018.

[16] F. Toso, M. Berto, L. Alberti, and F. Marcuzzi, "Efficient qr updating factorization for sensorless synchronous motor drive based on high frequency voltage injection," *IEEE Transactions on Industrial Electronics*, vol. 67, DOI 10.1109/TIE.2019.2959478, no. 12, pp. 10 213–10 222, Dec. 2020.

[17] J. Lee, Y. Kwon, and S. Sul, "Experimental identification of ipmsm flux-linkage considering spatial harmonics for high-accuracy simulation of ipmsm drives," in *2018 IEEE Energy Conversion Congress and Exposition (ECCE)*, DOI 10.1109/ECCE.2018.8558379, pp. 5804–5809, Sep. 2018.